Course 3

CAVITY QUANTUM ELECTRODYNAMICS

M. Brune

Laboratoire Kastler Brossel,
Ecole Normale Supérieure,
Paris, France

D. Estève, J.-M. Raimond and J. Dalibard, eds.
Les Houches, Session LXXIX, 2003
Quantum Entanglement and Information Processing
Intrication quantique et traitement de l'information

Contents

1. Introduction

One of the most important feature of quantum physics is the concept of entanglement. After interaction, two quantum objects usually behave as a single entity, each of the systems can not any more be described separately. A non-separable entangled state must the be introduced for representing the state of the system as a whole. Such a state presents unbelievable correlation from the point of view of classical logic as pointed out By Einstein Podolsky and Rosen [1] (EPR). Entanglement manifests while performing a measurement on one of the two parts of an EPR pair. It enforces to consider that the other part of the system is instantaneously projected during this measurement independently of the distance separating the two systems. The EPR situation also sits at the heart of quantum measurement theory. While describing quantum mechanically the interaction of a system with a meter, one have to consider at some point a system-meter entangled state whose strangeness was emphasized by the famous Schrödinger cat metaphor [2, 3]. While considering this problem the physics of entangled states provides a new insight in the understanding of the transition between the quantum word of small isolated quantum systems and the classical behavior of macroscopic meters. The concept of decoherence [4, 5], introduced in this context by considering the entanglement of the meter with its environment also relies on the understanding of the behavior of complex entangled states.

Beyond these fundamental problems, entanglement has also be more recently recognized as a powerful tool for manipulating information [6]. The emerging field of quantum information processing opens now the way to the use of entanglement for performing tasks that are impossible to achieve as efficiently with classical logic. Quantum cryptography [7] , whose inviolability relies on quantum physical rules, and teleportation [8] are the most spectacular achievement of this field. New perspectives now rely on advances in the manipulation of isolated particles allowing the preparation of tailored entangled states.

Various techniques are presently used for investigating quantum features related to entanglement in highly controlled systems. The key point is the degree of isolation of the system with respect to the environment. Pioneering experiments where performed with correlated photons. Once entangled, these particle propagate over large distances without interaction with the environment, thereby preserving entanglement until detection. Strongly entangled photon pairs are spontaneously produced by atomic cascades or parametric down-conversion. They have been used to demonstrate the violation of Bell inequalities [9, 10] as well as to implement quantum cryptography [11] and teleportation [12–14]. Triplets of entangled photons have also been generated and used for non-locality tests [15, 16]. This way of getting entangled particles relies however on random irreversible processes. In these experiments, one uses the entangled states that nature gives spontaneously in very specific situations. The method is thus limited to the demonstration of entanglement in relatively simple situations.

Progresses in the manipulation of single isolated massive particles have opened new perspectives by allowing to “synthesize" deterministically complex multi-particle entangled states. The key feature here is the use of strong interactions at the single particle level for generation of entanglement in controlled reversible Hamiltonian processes. Strongly interacting particles however, are also very often strongly coupled to the environment. The difficulty then consists in minimizing this coupling which is responsible for decoherence while preserving strong mutual interactions inside the system. This is presently achieved in two different fields: Ion trapping [17, 18] and microwave Cavity Quantum Electrodynamics (CQED) [19].

This course is devoted to the physics of entanglement in microwave CQED experiments. The heart of this system is a microwave photon trap, made of superconducting mirrors, which stores a few-photon field in a small volume of space for times as long as milliseconds. This field interacts with “circular" Rydberg atoms [20] injected one by one into the cavity. They combine a huge dipole coupling to a single photon with a lifetime (30 ms) three orders of magnitude larger than the cavity crossing time (20 μs). In this system, coupling to the environment is weak enough so that coherent atom-field interaction overwhelms dissipative processes achieving the so called “strong coupling regime". We will focus here on experiments where the strong coupling regime is used to built quantum gates in order to prepare complex multiparticle entangled states. The field of manipulation of *Schrödinger cat states* of the cavity field is investigated in details in the lecture by S. Haroche in this book.

Section 2 of this course is devoted to the description of the strong coupling regime in Rydberg atom CQED [21–24]. The tools of the experiment are briefly presented at the beginning of this section as well as the main characteristics of the strong coupling regime [25–27]. We then present in section 3, how to use the strong atom-cavity to perform various two particles quantum gates. The principle of operation of a quantum phase gate will be discussed. When associating this gate to arbitrary single qubit manipulation, one gets a universal set of gate allowing the step by step preparation of arbitrary multiparticle entangled states. In section 4, we will illustrate this ability by presenting an experimental preparation of a three particles GHZ (Greenberger Horne Zeilinger [15]) entangled state [28].

2. Microwave CQED experiments: The strong coupling regime

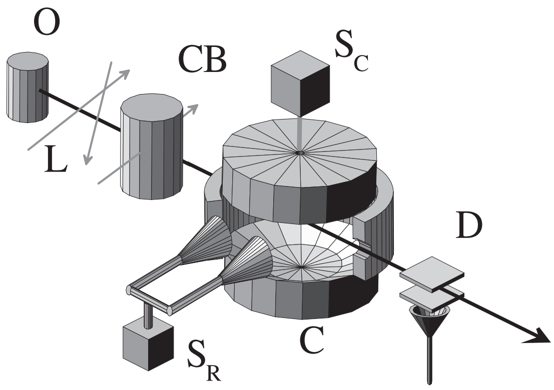

Fig. 1. Experimental set-up

The microwave CQED experiments described in this course all rely on the strong coupling between single two level atoms and a few microwave photons stored in a high Q superconducting cavity. We will recall here the essential properties of the various element of the setup as sketched in fig. 1. A thermal beam of Rubidium atoms originating from oven O is promoted to highly excited circular Rydberg states in the circularization box CB. The excitation scheme is made velocity-selective by a combination of velocity selective optical pumping performed by the lasers L and time of flight techniques [27]. The monokinetic atomic beam then crosses a high Q superconducting cavity mode C tuned close to transition between two circular levels e and g. A small classical field can be injected into C by the classical source S_C. Before and after interaction with C, the atoms can be exposed to microwave pulses generated by the source S_R. These pulses are used for preparation or detection of arbitrary two level superposition states. After leaving C, the atoms are detected one by one in a state selective ionization detector D allowing one to measure whether the atom eventually is in state e or g. Because of the use of superconducting material as well as to the high sensitivity of circular Rydberg atoms to blackbody radiation, all the elements of the set-up, from the circularization to the detection of the atoms, must be cooled down between 1.2 and 0.6 K in a ^{3}He cryostat.

2.1. The experimental tools and orders of magnitude

2.1.1. Circular Rydberg atoms

They combine a large principal quantum number N with maximal orbital and magnetic quantum numbers $l = |m| = N - 1$. A circular state with principal quantum number N will be referenced as N_c. The wavefunction of the Rydberg electron is a torus whose diameter is $a_0 N^2$. This “large" wavefunction results in a very large dipole coupling between adjacent circular levels. In the experiments described here, the levels e and g are respectively the 51_c and 50_c states. The dipole matrix element between these levels is $d = qa_0 N^2/2 = 1250\, a.u.$. The frequency of this transition is $\nu_{eg} = 51.099$ GHz.

The circular atomic levels are prepared by exciting the valence electron of Rubidium atoms into the 52_c state in a complex process involving 52 photons [20]. The 51_c or 50_c levels are then prepared selectively by a last microwave pulse resonant either on the $52_c \rightarrow 51_c$ one-photon or $52_c \rightarrow 50_c$ two-photon transition at 48.195 GHz and 49.647 GHz, respectively. This process prepares up to 400 circular atoms per preparation pulse. The selectivity of the last microwave transition in a large dc electric field allows the elimination of spurious elliptical levels (all other values of l and m). The purity of the prepared state, measured by a selective spectroscopic method is better than 98%. The stability of circular atoms requires the application of a small electric field providing a physical quantization axis everywhere in the set-up [29]. Under this condition, the atoms prepared in e or g behave as ideal long lived two level atoms while they interact with a nearly resonant cavity mode.

Circular atoms are easily detected by ionization in a relatively small static electric field. As the ionization threshold increases with the binding energy of the levels, one can selectively ionize either e or g in two different detectors. This detection scheme, relies on electron counting. It is extremely sensitive and behave as a meter for the energy of a single atom. It allows measurements on a single realization of the experiment as well as to measure average values of the atomic energy by resuming the same experiment until significant statistics is obtained. The regime of single atom interaction with the cavity is achieved at the expense of low counting rates of typically 0.1 to 0.2 detected atom per preparation pulse (detection efficiency 40%(10)). In this limit, the Poissonian statistic of the number of excited atoms results in a negligible probability to excite two atoms at the same time.

A pulsed velocity selective optical pumping scheme prepares monokinetic Rubidium atoms [27] in the state $5s_{1/2}\ F = 3$ just after they leave the oven O. This level is the starting point of the circular atoms preparation. The width of the velocity distribution obtained in this way is 10 m/s. It is reduced to 1.5 m/s by time of flight selection between optical pumping and circularization which is also a pulsed process. Due to the control of the atomic velocity and of the time of preparation of Rydberg atoms, one knows the position of the circular atoms inside the setup with a precision of $\pm 1\ mm$. This is used for applying to each atom the proper sequence of controlled interactions with the cavity mode and the auxiliary classical microwave pulses. In particular, the atom-cavity interaction time is adjusted by switching on and off an electric field of about 1 V/cm between the cavity mirrors. The atoms are then tuned in and out of resonance by Stark effect at user controlled programmable times while they cross the cavity.

2.1.2. *The photon box*

The cavity is made of two massive Niobium mirrors in a Fabry-Perot geometry depicted in fig. 1. The two spherical mirrors have a radius of curvature of 40 mm. The distance between the mirrors at center is 27.5 mm. The atoms are nearly resonantly coupled to the TEM_{900} Gaussian mode whose resonance frequency is close to $\nu_{eg} = 51.099\ GHz$. The mode waist, $w_0 = 5.96\ mm$, is close to the wavelength, $\lambda = 6\ mm$. The corresponding mode volume [21] is relatively small ($V \simeq 700\ mm^3$). The microwave electric field amplitude at cavity center $E_0 = \sqrt{h\nu_{eg}/2\epsilon_0 V} = 1.5\ mV/m$ is the essential parameter characterizing the coupling with the atomic dipole. Due to geometrical defects of the mirrors, the degeneracy between the two modes with linear perpendicular polarizations is lifted by about 100kHz. When one atom interacts resonantly with one of these two modes, the coupling with the other one usually plays a negligible role.

A quality factor as high as 3.10^8 corresponding to a photon lifetime of 1 ms is obtained by careful polishing and processing of the mirrors. It is limited by diffusion of photons out of the aperture between the mirrors due to the residual roughness of their surface. These losses do not occur in a closed cavity [30]. However, the closed geometry is not compatible with the electric field needed for stabilizing circular atoms [29]. Diffusion losses are reduced by inserting an aluminum ring nearly closing the opening between the mirrors. The atoms enter the cavity trough 3 mm diameter holes in this ring. Inhomogeneous electric fields in these holes destroy atomic coherence but they do not affect the populations of Rydberg states. An external microwave source is coupled into the cavity mode through small 0.2 mm diameter holes at the center of the mirrors.

2.2. *Resonant atom-field interaction: The vacuum Rabi oscillation*

A detailed description of the atom-cavity interaction can be found in various review papers [21–24] as well as in the lecture by S. Haroche. It relies on the Jaynes-Cummings hamiltonian [31] whose eigenstates are the so called “dressed states" [32] of the atom-field system. The non-degenerate ground state of the system is $|g, 0\rangle$ where 0 stands for the photon number. We are interested here in the dynamics of the two first excited states of the system $|g, 1\rangle$ and $|e, 0\rangle$ which are coupled by an electric dipole transition. This coupling results in a splitting $\hbar\Omega_0 = -2dE_0$ of the first dressed states $|+, 0\rangle$ and $|-, 0\rangle$. An atom initially in state e crossing an empty cavity thus experiences a “vacuum Rabi oscillation": Atom and field exchange periodically one photon at the Rabi frequency $\Omega_0/2\pi = 47\,kHz$.

The corresponding Rabi oscillation signal [26] is presented in fig. 2. It shows the measured average atomic excitation as a function of the atom-field interaction time. The cavity is tuned at resonance with the 51_c to 50_c transition. The mode Q factor is 7.10^7, corresponding to a photon lifetime of 220 μs. Up to four cycles of Rabi oscillations are clearly observed demonstrating the strong coupling regime. The decay of the oscillation signal is due to various imperfections (dark counts, atoms detected in the wrong channel, inhomogeneous stray electric or magnetic fields).

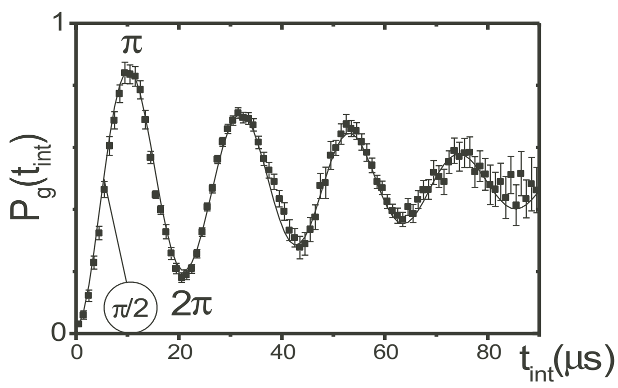

Fig. 2. Rabi oscillation signal: A single atom emits and reabsorbs a single photon. Up to 4 oscillation cycles are observed. Interaction times corresponding to $\pi/2$, π and 2π pulses are marked by labels

If the cavity contains initially n photons, the Rabi oscillation frequency become $(\Omega_0/2\pi)\sqrt{n+1}$ [33]. By observing the Rabi oscillation in a small coherent field [34] stored in C, a discrete spectrum of Rabi frequencies has been observed [22,26]. Note that this spectrum is a direct manifestation of field energy quantization in the cavity mode. This feature has also been used for measuring the photon number distribution of small coherent fields stored in C with up to 1.4 photons o, average [26]. Rabi oscillation in small photon number states was also observed in [35].

More recently, the Rabi oscillation in a coherent field has been used to generate phase "Schrödinger cat states" involving fields containing up to 40 photons [36]. The method of preparation and detection of such states is presented in section 2 of the course By S. Haroche in this book.

3. "Quantum logic" operations based on the vacuum Rabi oscillation

The vacuum Rabi oscillation provides important tools for implementing quantum gates performing basic two qubit logic operations.In this section, we briefly present these basic operations. In the next section we will show how they can be combined in order to engineer step by step a three qubit entangled state.

For an atom and a field initially prepared either in $|e, 0\rangle$ or $|g, 1\rangle$, the atom-field wavefunctions after the interaction time t_{int} read respectively :

$$|\psi_e(t_{int})\rangle = cos(\Omega_0 t_{int}/2)|e, 0\rangle + sin(\Omega_0 t_{int}/2)|g, 1\rangle \tag{3.1}$$

$$|\psi_g(t_{int})\rangle = cos(\Omega_0 t_{int}/2)|g, 1\rangle - sin(\Omega_0 t_{int}/2)|e, 0\rangle \tag{3.2}$$

Three basic functions are realized by adjusting the atom-cavity interaction time to specific values corresponding to $\Omega_0 t_{int} = \pi/2, \pi$ or 2π. The π pulse can be used to exchange one excitation between the atom and the cavity mode. In this way, an atom in e can be used to *write* a one-photon field in the cavity. If the atom is prepared in the arbitrary superposition state $c_e|e\rangle + c_g|g\rangle$, it will, after a π pulse, always end up in g and prepare the field in the state: $c_e|1\rangle + c_g|0\rangle$. All the quantum information encoded in the atom by a classical microwave pulse is transferred and stored in the cavity. This writing process being reversible, the stored quantum information can be *read* by another atom prepared in g which is performing an absorbing π pulse. In these processes, the cavity acts as a quantum memory as demonstrated in [27].

In case of an atom prepared in e performing $\pi/2$ pulse in the cavity, the prepared atom-field state is:

$$|\psi_{EPR}\rangle = 1/\sqrt{2}(|e, 0\rangle + |g, 1\rangle) \tag{3.3}$$

It is a maximally entangled state analogous to the singlet state of a pair of spin $1/2$. As the atom leaves the cavity after interaction, this state exhibits the non-local quantum correlations which are at the heart of the EPR [1] situation and which characterize vividly the difference between quantum and classical logic through the Bell theorem [9]. Preparation and characterization of $|\psi_{EPR}\rangle$ is presented in [37].

Let us finally consider the 2π Rabi pulse. When the atom is prepared in g the atom-field wavefunction transforms in the following way:

$$\begin{array}{lcl} |g, 1\rangle & \rightarrow & -|g, 1\rangle \\ |g, 0\rangle & \rightarrow & |g, 0\rangle \end{array} \tag{3.4}$$

For a field containing one photon, the 2π pulse leads to a π phase shift of the atom-field state as seen on eq. 3.4. A similar π–phase shift occurs when performing a 2π rotation on a spin 1/2 system [38, 39]. Now if the cavity is initially empty, the system is in the ground state $|g, 0\rangle$. It does not evolve and does not experience any phase shift. In both cases, the field energy (i.e. 0 or 1 photon) is unchanged but the phase of the final state carries information on the photon number. This provides the principle of the QND (quantum non demolition) method of measurement of a 0 or 1 photon field discussed in details in [40].

It also allows one to implement the so cold *Quantum Phase Gate* (QPG) [41]. When combined with arbitrary single qubit operations (i.e. classical microwave pulses applied to single atoms) this two qubits gate is equivalent to the CNOT gate and plays the role of a universal gate for *synthesizing* arbitrary N qubits entangled states.

The QPG transformation simply reads:

$$|a, b\rangle \longrightarrow \exp(i\phi\delta_{a,1}\delta_{b,1})|a, b\rangle \tag{3.5}$$

where $|a\rangle$, $|b\rangle$ stand for the basis states ($|0\rangle$ or $|1\rangle$) of the two qubits and $\delta_{a,1}$, $\delta_{b,1}$ are the usual Kronecker symbols. The QPG leaves the initial state unchanged, except if both qubits are 1, in which case the state is phase–shifted by an angle ϕ. In order to implement the QPG, let us now consider a third atomic level i and let us assume that due to large detunings, this level is not coupled to the high Q cavity mode. To be specific let us consider i as the circular Rydberg state with principal quantum number $N_c = 49$. The transformation corresponding to the 2π Rabi pulse in C is:

$$\begin{array}{ccc} |i, 0\rangle & \longrightarrow & |i, 0\rangle \\ |i, 1\rangle & \longrightarrow & |i, 1\rangle \\ |g, 0\rangle & \longrightarrow & |g, 0\rangle \\ |g, 1\rangle & \longrightarrow & -|g, 1\rangle \end{array} \tag{3.6}$$

When mapping the atomic states i and g on the logical 0 or 1 value of the atomic qubit, it exactly realizes the $\phi = \pi$ QPG. The ability of this gate to generate entangled states can be demonstrated by operating it on a superposition state of either the atomic or field qubit. As an exemple, after preparing the atom-field in the state $1/2(|i\rangle+|g\rangle)(|0\rangle+|1\rangle)$ the operation of the QPG prepares the maximally entangled state:

$$1/2(|i\rangle + |g\rangle)|0\rangle + (|i\rangle - |g\rangle)|1\rangle) \tag{3.7}$$

This equation shows that after interaction with C, the atomic state superposition is phase shifted by π if and only if the cavity contains one photons. Note that the 2π pulse interaction with C leaves the photon number unchanged. Measuring the phase of the atomic superposition state thus amounts to a Quantum Non Demolition (QND) detection of a single photon in C. As shown in [40], this atomic measurement can be implemented using a Ramsey interferometer by applying classical $\pi/2$ pulses to the $g - i$ transition before and after the atom crosses C. This experiment demonstrates that the phase of an atomic superposition state is coherently controlled by the state of a single photon. Symmetrically, we have also demonstrated that the phase of a superposition of the 0 and 1 field states is shifted by π under the operation of the QPG when the atom is prepared in g [41].

4. Step by step synthesis of a three particles entangled state

We present now an experiment where we prepare a set of three entangled qubits consisting of two atoms and a 0 or 1 photon field stored in C [28] by combining elementary quantum gate operations. It is the first example of preparation of a tailored three particle entangled state by a programmed sequence of quantum gates.

4.1. Principle of the preparation of the state

We first recall the sequence of operations used to prepare the three particle entangled state. It was proposed independently in [42] and [43]. The corresponding timing is sketched fig. 3.a. We send across C, initially empty, an atom A_1 initially in e. A $\pi/2$ Rabi pulse prepares the state $|\psi_{EPR}\rangle$ described by eq. 3.3. We then send a second atom A_2. Initially in g, it is prepared, before C, in the state $(|g\rangle + |i\rangle)/\sqrt{2}$ by a Ramsey pulse P_2. This atom interacts with C during its full cavity crossing time (2π Rabi pulse) and performs the QPG operation. Using eq. 3.6, the resulting $A_1 - A_2 - C$ quantum state is :

$$|\Psi_{triplet}\rangle = \frac{1}{2}\left[|e_1\rangle(|i_2\rangle + |g_2\rangle)|0\rangle + |g_1\rangle(|i_2\rangle - |g_2\rangle)|1\rangle\right] \tag{4.1}$$

(the state indices correspond to the atom number). Eq. 4.1 describes a three particle entangled state and can be rewritten as :

$$|\Psi_{triplet}\rangle = \frac{1}{2}\left[|i_2\rangle(|e_1, 0\rangle + |g_1, 1\rangle) + |g_2\rangle(|e_1, 0\rangle - |g_1, 1\rangle)\right] \ , \tag{4.2}$$

describing an $A_1 - C$ EPR pair whose phase is conditioned to the A_2 state. Since $|\Psi_{triplet}\rangle$ involves two levels for each subsystem, it is equivalent to an entangled state of three spins 1/2. Let us define the states $|+_i\rangle$ $(|-_i\rangle)$ (with $i = 1, 2$) as $|+_1\rangle = |e_1\rangle$ $(|-_1\rangle = |g_1\rangle)$, $|\pm_2\rangle = (|g_2\rangle \pm |i_2\rangle)/\sqrt{2}$ and $|+_C\rangle = |0\rangle$ $(|-_C\rangle =$

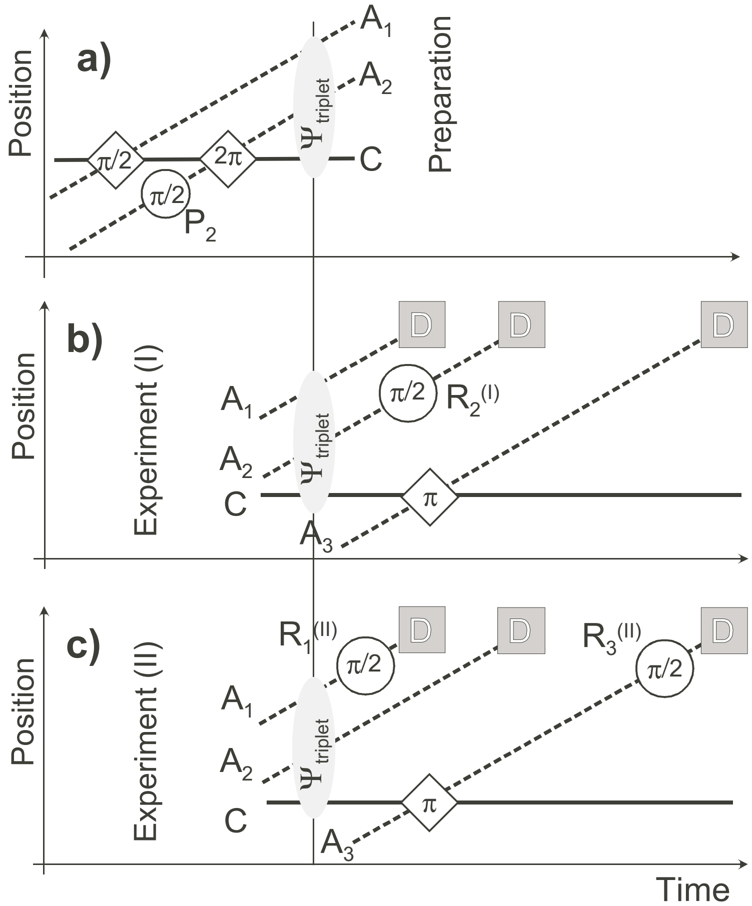

Fig. 3. The entanglement procedure. Qualitative representation of the atoms and cavity space lines during the experiments. The diamonds depict the atom-cavity interactions and the circles the classical pulses produced by S_R. The dark squares are the detection events. a) Preparation of the entangled state $|\Psi_{triplet}\rangle$ sketched by the grey oval. b) Experiment (I): Detection of “longitudinal" correlations. c) Experiment (II): Detection of “transverse" correlations.

$|1\rangle$). With these notations, $|\Psi_{triplet}\rangle$ takes the form of the Greenberger, Horne and Zeilinger (GHZ) spin triplet [15]:

$$|\Psi_{triplet}\rangle = \frac{1}{\sqrt{2}}\left(|+_1, +_2, +_C\rangle - |-_1, -_2, -_C\rangle\right) , \tag{4.3}$$

Other schemes have been proposed to realize many particle atom-cavity entanglement [44,45].

4.2. Detection of the three-particle entanglement

In order to characterize the state $|\Psi_{triplet}\rangle$, we are able to detect the atomic energy states, but not directly the cavity field. It can, however, be copied onto a third atom A_3 and detected afterwards [27]. The $A_3 - C$ interaction is set so that A_3, initially in g, is not affected if C is empty, but undergoes a π Rabi pulse in a single photon field : $|g, 0\rangle \rightarrow |g, 0\rangle$ and $|g, 1\rangle \rightarrow -|e, 0\rangle$. Within a phase, A_3 maps the state of C. Thus, by detecting A_1, A_2 and A_3, we measure a set of observable belonging to the three parts of the entangled triplet. If A_3 crosses C before A_1 exits the ring, a three-atom entangled state $|\Psi'_{triplet}\rangle$ would be created between these two events :

$$|\Psi'_{triplet}\rangle = \frac{1}{2}\left[|e_1\rangle(|i_2\rangle + |g_2\rangle)|g_3\rangle - |g_1\rangle(|i_2\rangle - |g_2\rangle)|e_3\rangle\right] \tag{4.4}$$

$$= \frac{1}{2}\left[|i_2\rangle(|e_1, g_3\rangle - |g_1, e_3\rangle) + |g_2\rangle(|e_1, g_3\rangle + |g_1, e_3\rangle)\right] \tag{4.5}$$

Even if A_3 is delayed, its correlations with A_1 and A_2, which reflect those of C, are the same as those described in eq. 4.5. In the following discussion, we thus refer equivalently to C or A_3.

Checking the $A_1 - A_2 - C$ entanglement involves measurements in two different bases. A microwave pulse, after the interaction with C, followed by energy detection in D allows us to probe each atom's pseudo-spin along an arbitrary "quantization axis". In a first experiment (I), whose timing is sketched fig. 3.b, we check "longitudinal" correlations by detecting the "spins" along what we define as the "z axis" (eigenstates $|\pm_i\rangle$ for $i = \{1, 2\}$ and $|+_3\rangle = |e_3\rangle$ and $|-_3\rangle = |g_3\rangle$ for A_3). For A_1 and C (i. e. A_3), this is a direct energy detection. For A_2, a $\pi/2$ analysis pulse $R_2^{(I)}$ on the $i \rightarrow g$ transition transforms $|+_2\rangle$ (resp. $|-_2\rangle$) into $|i_2\rangle$ (resp. $|g_2\rangle$). The three atoms should thus be detected in $\{e_1, i_2, g_3\}$ or $\{g_1, g_2, e_3\}$, with equal probabilities. However, these correlations, taken alone, can be explained classically (statistical mixture of $|e_1, i_2, g_3\rangle$ and $|g_1, g_2, e_3\rangle$ states).

A second experiment (II) is required to test the quantum nature of the superposition. We study "transverse correlations" by detecting A_1 and A_2 along the "x axis" (eigenstates $|\pm_{x,i}\rangle = (|+_i\rangle \pm |-_i\rangle)/\sqrt{2}$). A_3 is detected along an axis in the horizontal plane at an angle ϕ from the x direction (eigenstates $|\pm_{\phi,i}\rangle = (|+_i\rangle \pm \exp(+i\phi)|-_i\rangle)/\sqrt{2}$). The timing of experiment (II) is sketched fig. 3.c. Atom A_2 is directly detected in D, since $|\pm_{x,2}\rangle$ coincide with $|g_2\rangle$ and $|i_2\rangle$. A_1 and A_3 undergo, after C, two analysis $\pi/2$ pulses $R_1^{(II)}$ and $R_3^{(II)}$ on the $e \rightarrow g$ transition, with a phase difference ϕ. A detection in g amounts to a detection in $|+_x\rangle$ or $|+_\phi\rangle$ for A_1 and A_3 respectively at the exit of C.

For sake of clarity, let us first consider the case of only two atoms (1 and 3) in state:

$$|\Psi'_{EPR}\rangle = \frac{1}{\sqrt{2}}(|e_1, g_3\rangle - |g_1, e_3\rangle) . \tag{4.6}$$

These atoms are analyzed along the x and ϕ directions respectively. When A_1 is detected in $|+_{x,1}\rangle$ (i. e. g_1 in D), A_3 is projected onto $|-_{x,3}\rangle$, since $|\Psi'_{EPR}\rangle$ is the rotation-invariant spin singlet. The detection probability of A_3 in $|+_{\phi,3}\rangle$ (i. e. g_3 in D) thus oscillates versus ϕ between 1 for $\phi = \pm\pi$ and 0 for $\phi = 0, 2\pi$: "Fringes" observed in the joint detection probabilities of the two atoms [37] show that quantum coherence has been transferred between them through the EPR correlations. The phase of the fringes would be shifted by π if the minus sign in eq. 4.6 was changed into a plus. Returning to the three system case, eq. 4.5 shows that similar fringes are expected for the joint detection of A_1 and A_3 corresponding to a given state for A_2. They have the same phase as the EPR fringes described by eq. 4.6 when A_2 is in i_2. They are shifted by π when A_2 is in g_2. This shift results from the action of the $A_2 - C$ phase gate [41] on the $A_1 - C$ EPR pair.

A tight timing is required to have A_1 and A_2 simultaneously inside the ring so that $|\psi_{triplet}\rangle$ is prepared before A_1 losses its coherence in the exit hole of the cavity (it was not the case in the experiments described in section 3.4). A_2 interacts with C for the full atom−cavity interaction time. The π Rabi pulse condition for A_3 is realized with the Stark switching technique. Atom A_1 couples to C 75 μs after the erasing sequence, and should undergo a $\pi/2$ Rabi rotation. It is followed by A_2 after a delay of 25 μs. The separation between A_1 and A_2 is 1.2 cm, twice the cavity waist. Nevertheless, A_1 still interacts with C when A_2 starts its 2π Rabi rotation. Even in this case, an appropriate adjustment of the atom cavity Stark tuning allows to prepare $|\psi_{triplet}\rangle$ with a high fidelity as shown in [28]. Atom A_1 has exited the ring however before A_3 has crossed C, following A_2 after a delay of 75 μs. This timing thus does not permit to prepare $|\Psi'_{triplet}\rangle$ (eq. 4.5). As discussed above, the $A_1 - A_2 - A_3$ correlations nevertheless demonstrate the $A_1 - A_2 - C$ entanglement.

We apply the classical $\pi/2$ microwave pulses when the atom is in an antinode of the standing wave created inside the cavity ring by a classical microwave source S_R. The distance between A_1 and A_2 is such that one is in a node of this wave when the other is in an antinode. In this way, selective pulses may be applied on A_1 and A_2 even if both are simultaneously in the ring. In experiment (I), P_2 and $R_2^{(I)}$ are applied on A_2 on the 54.3 GHz $g \rightarrow i$ transition. In experiment (II), $R_1^{(II)}$ and $R_3^{(II)}$ are used to probe the $|\pm_{x,1}\rangle$ and $|\pm_{\phi,3}\rangle$ states. A pulse resonant on the $e \rightarrow g$ transition would couple in C through scattering on the mirrors imperfections. A field would then build up in C and spoil quantum correlations. To avoid this, we first apply a π pulse on the $g \rightarrow i$ transition transforming the $e-g$ coherence into an $e-i$ one. A $\pi/2$ pulse on the two-photon $e \rightarrow i$ transition at 52.7 GHz, which does not feed any field in C, is then used to probe this coherence. States $|+_{x,1}\rangle$ ($|-_{x,1}\rangle$) and $|+_{\phi,3}\rangle$ ($|-_{\phi,3}\rangle$) are mapped by this effective three-photon $\pi/2$ pulse onto i_1 (e_1) and i_3 (e_3) respectively. The results

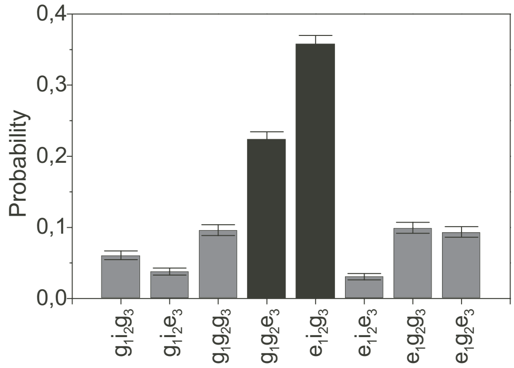

Fig. 4. Longitudinal correlations (experiment I). Histograms of the detection probabilities for the eight relevant detection channels. The two expected channels (g_1, g_2, e_3 and e_1, i_2, g_3, black bars) clearly dominate the others (grey bars), populated by spurious processes. The error bars are statistical.

of experiment (I), fig. 4, are presented as histograms giving the probabilities for detecting the atoms in the eight relevant channels. As expected, the $\{e_1, i_2, g_3\}$ and $\{g_1, g_2, e_3\}$ channels dominate. The total probability of these channels is $P_\parallel = 0.58 \pm 0.02$. The difference between them is due to experimental imperfections. Channel $\{g_1, g_2, e_3\}$ corresponds to one photon stored in the cavity between A_1 and A_3. It is thus sensitive to field relaxation, and leaks into the other $\{g_1\}$ channels. Events with two atoms in the same sample, residual thermal fields, detection errors also contribute to the population of the parasitic channels. Note also that since the experiment involves three levels for each atom, there are altogether 27 detection channels. Fig. 4 presents the channels corresponding to the relevant transitions for each atom: $e \rightarrow g$ for A_1 and A_3 ; $g \rightarrow i$ for A_2.

The other channels are weakly populated by spurious effects (spontaneous emission outside C, residual thermal photons, influence of the $R_3^{(I)}$ or P_2 pulses on the other atoms, absorption of the cavity field by A_2 due to imperfect 2π Rabi rotation..). The total contribution of these transfer processes is below 15%.

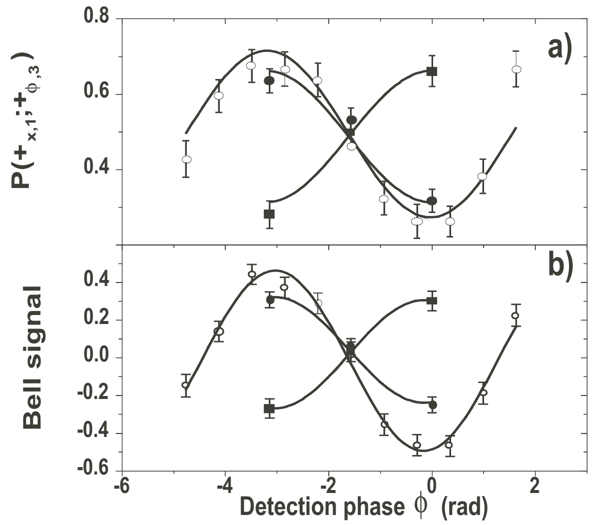

Fig. 5. transverse correlations (experiment II).

For the signals of experiment (II) presented on fig. 5, the relative phase ϕ of $R_3^{(II)}$ and $R_1^{(II)}$ is adjusted by tuning the frequency of the source inducing the $e \rightarrow i$ two-photon transition. Fig. 5.a presents versus ϕ the probability $P(+_{\phi,3};+_{x,1})$ for detecting A_3 in i (i. e. $|+_{\phi,3}\rangle$) provided A_1 has also been detected in i (i. e. $|+_{x,1}\rangle$). The open circles give the conditional probability when A_2 is not sent. The observed fringes correspond to the two-atom EPR pair situation. The solid circles give the corresponding conditional probability when A_2 is detected in i. Due to very long acquisition times (eight hours for the data in fig. 5), signals have been recorded only for three phase values. The squares correspond to a detection of A_2 in g. The $A_1 - A_3$ correlations are not modified when A_2 is detected in i. When A_2 is detected in g, the $A_1 - A_3$ EPR fringes are shifted by π, as expected. All joint probabilities corresponding to the four possible outcomes for A_1 and A_3 are combined to produce the "Bell signal" [10] which is the expectation value $\langle\sigma_{x,1}\sigma_{\phi,3}\rangle = P_{i_1,i_3} + P_{e_1,e_3} - P_{i_1,e_3} - P_{e_1,i_3}$, where the σ's are Pauli matrices associated to the pseudo-spins and P_{a_1,b_3} is the probability for detecting A_1 in a and A_3 in b ($\{a, b\} = \{i, e\}$). We plot fig. 5.b the Bell signal versus ϕ. The open circles correspond again to no A_2 atom sent, the solid circles and squares to A_2 detected in i or g, respectively. The π phase shift of the $A_1 - A_3$ EPR correlations, conditioned to the A_2 state, is conspicuous. The fringes visibility is $2V_{\perp} = 0.28 \pm 0.04$.

Due to experimental imperfections, the first stage fig. 3.a of our experiment does not prepare the pure state $|\Psi_{triplet}\rangle$, but rather a mixed state described by a density matrix ρ. The set-up efficiency is thus characterized by a fidelity $F = \langle\Psi_{triplet}|\rho|\Psi_{triplet}\rangle$. If the detection stages (fig. 3.b and 3.c) were perfect, F would be equal to the sum $P_{\parallel}/2 + V_{\perp}$ [18]. The value of this quantity, 0.43, is however affected by known detection errors and F is actually larger. Trivial imperfections can occur at three different stages: The mapping of the cavity state onto A_3, the classical microwave pulses $R_2^{(I)}$, $R_1^{(II)}$ and $R_3^{(II)}$, and the energy state-selective atom counting. We have determined these errors independently by additional single atom experiments. Taking them into account, we determine a fidelity $F = 0.54 \pm 0.03$. The three kinds of errors listed above account respectively for corrections of 0.03, 0.05 and 0.03 to the raw 0.43 value. The fact that F is larger than 0.5 ensures that genuine three particle entanglement is prepared here [18].

The combined results of experiments (I) and (II) demonstrate the step by step engineered entanglement of three qubits, manipulated and addressed individually. By adjusting the various pulses, the experiment could be programmed to prepare other tailored multiparticle state. In particular, the generalization of our experiment for preparing multiparticle generalizations of the GHZ triplet [46] are straightforward. These states are generated by a simple iteration of the present scheme [43, 44]. After having prepared the $A_1 - C$ pair in the state described by eq. 4.1, one sends a stream of atoms $A_2 - A_3 - \cdots - A_n$ all prepared in $(|i\rangle + |g\rangle)/\sqrt{2}$ and undergoing, if in g, a 2π Rabi rotation in a single photon field. Since this rotation does not change the photon number, the 0 photon (resp. 1 photon) part of the $A_1 - C$ system gets correlated to an $A_2 - A_3 - \cdots - A_n$ state with all $n-1$ atoms in $(|i\rangle + |g\rangle)/\sqrt{2}$ (resp $(|i\rangle - |g\rangle)/\sqrt{2}$), preparing the entangled state :

$$|\Psi\rangle = \frac{1}{\sqrt{2}}\left(|+_1, +_2, \cdots, +_C\rangle - |-_1, -_2, \cdots, -_C\rangle\right) \ . \qquad (4.7)$$

This state presents non–local $n+1$ particles correlations which could be investigated by the techniques presented here.

Similar controlled and reversible manipulations of many particle entanglement can be performed with other systems. Complex spin manipulations have been demonstrated with nuclear magnetic resonance [47]. These experiments involve however macroscopic samples near thermal equilibrium without clear-cut entanglement [48]. Reversible entanglement with massive particles has also been realized with trapped ions [49]. The generation of an EPR pair [50] and, recently, of four ion entanglement [18] have been reported. In these experiments, strong coupling requires the ions to be only a few micrometers apart and the difficulty is to address them individually. The entangled multi-particle state is prepared in a collective process, involving all qubits at once. Individual addressing of ions is possible in larger ions traps as demonstrated with calcium [51] but controlled quantum logic operations have not yet been demonstrated in this context. In contrast to ion traps, our CQED experiment manipulates particles at centimeter-scale distances, ideal conditions for separate qubit control.

5. Direct atom-atom entanglement: cavity-assisted collisions

The atom-atom entangling procedures outlined above rely on the exchange of a photon between the atom and the cavity. The quantum information is transiently stored as a superposition of the zero and one photon states. These schemes are thus sensitive to cavity losses, the main cause of decoherence in our experiments (the atomic lifetime being much longer than the cavity damping time).

It is possible to circumvent this problem by entangling two atoms directly, in a collision process assisted by the non-resonant cavity modes [52]. The first atom (A_1) is initially in e and the second (A_2) in g. The atoms have now different velocities, so that the second catches up the first at cavity center, before exiting first from C. The two cavity modes M_a and M_b are now detuned from the $e \rightarrow g$ transition frequency by amounts Δ and $\Delta + \delta$, greater than Ω. Due to energy conservation, real photon emission cannot occur in this case. Atom A_1 can, however, virtually emit a photon immediately reabsorbed by A_2. This leads to a Rabi oscillation between states $|e, g\rangle$ and $|g, e\rangle$ and thus to atom/atom entanglement generation for most interaction times.

The situation is reminiscent of a resonant van der Waals collision in free space, which can also produce atom-atom entanglement for small enough impact parameters [53]. In the present case, the detuned cavity modes considerably enhance the atom-atom interaction. Note that, in this peculiar “collision" process, the actual distance between the atoms is irrelevant, provided they both interact with the modes.

The quantum amplitudes associated to states $|e, g\rangle$ and $|g, e\rangle$ are periodic functions of the collision duration (which depends on the atomic velocities). The oscillation frequency associated to this second order collision process is $(\Omega^2/4)[1/\Delta + 1/(\Delta + \delta)]$. By repeating the experiment, we reconstruct the probabilities P_{eg} and P_{ge} for finding finally the atom pair in states $|e, g\rangle$ and $|g, e\rangle$. We plot these probabilities versus the dimensionless parameter $\eta = \omega[1/\Delta +$

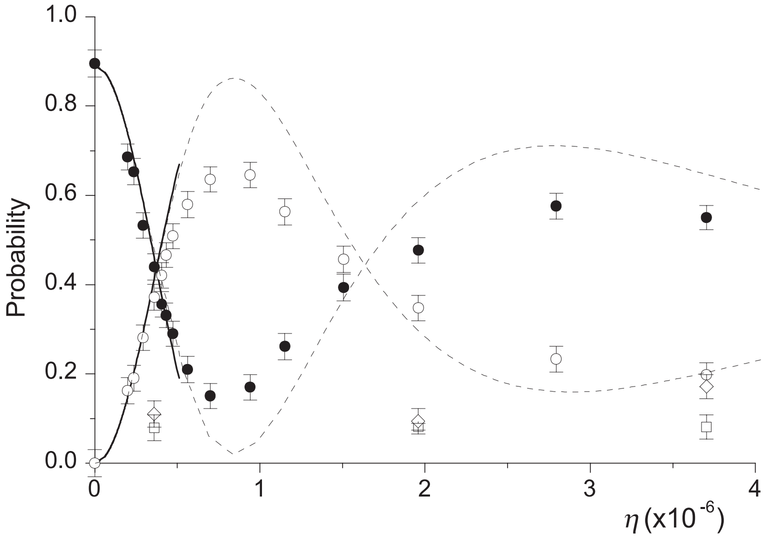

Fig. 6. Cavity assisted collision. Joint detection probabilities P_{eg} and P_{ge} versus the parameter η. Points are experimental. Solid lines for small η values correspond to a simple analytical model based on second order perturbation theory. The dashed lines (large η) present the results of a numerical integration of the system evolution (adapted from [52])

$1/(\Delta + \delta)$] (see Fig. 2). The oscillations of P_{eg} and P_{ge} as a function of η are well accounted for by theoretical models (solid and dashed lines in Fig. 2).

We have realized the situation of maximum entanglement by adjusting η to the value corresponding to $P_{eg} = P_{ge} = 0.5$. As for the sequential EPR pair generation scheme presented above, we have checked the coherent nature of the pair by performing measurements of observables whose eigenstates are superpositions of energy states.

Since this entanglement procedure implies only a virtual photon exchange with the detuned cavity mode, it is, in first order, insensitive to the cavity damping time or to a stray thermal field in the cavity modes. It thus opens interesting perspectives for demonstrating elementary steps of quantum logic with moderate Q cavities at finite temperature.

We have shown theoretically that the two-qubit Grover search algorithm [54] could be realistically implemented in our set-up with two cavity-assisted collisions between two atoms, performed during the common interaction of the atoms with the cavity mode [55].

6. Conclusion and Perspectives

The circular Rydberg atoms already made it possible to operate interesting quantum entanglement processing sequences. The extension to much more complex algorithms requires some improvements of the present set-up.

The fidelity is limited by the imperfections of the elementary gates and by the cavity losses. A better control of the stray fields in the set-up, which seem to be a major cause of imperfections, could improve noticeably this fidelity. The cavity losses could be reduced with a new mirror technology. Encouraging tests indicate that longer cavity damping times are realistically within reach. Moreover, the cavity-assisted collision process makes it possible, in principle, to realize high-fidelity quantum gates with a moderate quality factor.

The main limitation to the scalability thus appears to be the atomic preparation scheme. As discussed above, we operate with single atom samples at the expense of data taking times growing exponentially with the number of qubits. A recent improvement of the field ionization detector efficiency will allow us to run sequences with four or five atomic samples within realistic times.

Further extensions require a deterministic preparation of single Rydberg atom samples. The “dipole blockade" mechanism is a very promising tool [56]. In a dense sample of ground state atoms, the frequency of the transition between a one- and a two-Rydberg sample is displaced by a great amount from the transition producing the first Rydberg, due to the very strong dipole-dipole interaction between these atoms. The laser excitation thus produces a single Rydberg state, with a high probability. This low angular momentum state can be efficiently transferred later to the circular state. We are now developing an experiment based on “atom chips" [57] techniques to explore the feasibility of a deterministic Rydberg atom preparation.

This “atom pistol" would make complex sequences accessible. The maximum number of operations foreseeable is of the order of the atomic lifetime (30 ms) divided by the gate time (10 to 30 μs). This sets a fundamental limit of a few thousand quantum operations. This is far from what is required for a massive quantum computation with error correction. This number of operations is nevertheless competitive with other techniques and large enough to test interesting quantum algorithms and error correction procedures.

Let us note also that these experiments are well-suited to the exploration of other basic quantum mechanisms essential for quantum information processing. In particular, mesoscopic coherent fields stored in the cavity provide an unprecedented tool for an in-depth study of the decoherence mechanisms [36, 58]. We are envisioning an experiment with two superconducting cavity. This opens the way to the generation of non-local mesoscopic states (EPR pairs made of mesoscopic cavity fields) and allows new tests of our understanding of the decoherence process.

References

[1] A. Einstein, B. Podolosky and N. Rosen, Phys. Rev. **47**, 777 (1935).

[2] E. Schrödinger, Naturwissenschaften, **23**, 807, 823, 844 (1935); reprinted in english in [8].

[3] J.A. Wheeler and W.H. Zurek, *Quantum Theory of Measurement*, Princeton Univ. Press (1983).

[4] W.H. Zurek, Physics Today, **44**, 10 p. 36 (1991).

[5] W.H. Zurek, Phys. Rev. D **24**, 1516 (1981) and **26**, 1862 (1982); A.O. Caldeira and A.J. Leggett, Physica A **121**, 587 (1983); E. Joos and H.D. Zeh, Z. Phys. B **59**, 223 (1985); R. Omnès, *The Interpretation of Quantum Mechanics*, Princeton University Press, (1994).

[6] C. H. Bennett, D. P. DiVincenzo, Nature, **404**, 247 (2000).

[7] C. H. Bennett, G. Brassard, A. Ekert, Scientific American, October 1992, p.50.

[8] C. H. Bennett, G. Brassard, C. Crepeau, R. Jozsa, A. Peres, W.K. Wootters, Phys. Rev. Lett. **70**, 1895 (1993).

[9] J.S. Bell, Physics**1**, 195 (1964); J. F. Clauser, M. A. Horne, A. Shimony, R. A. Holt, Phys. Rev. Lett. **23**, 880 (1969).

[10] A. Zeilinger, Rev. Mod. Phys. **71**, S288 (1998).

[11] J. G. Rarity, P. C. M. Owens, P. R. Tapster, J. Mod. Opt. **41**, 2435 (1994).

[12] D. Bouwmeester, Pan Jian-Wei, K. Mattle, M. Eibl, H. Weinfurter, A. Zeilinger, Nature, **390**, 575 (1997).

[13] D. Boschi, S. Branca, F. De Martini, L. Hardy, S. Popescu, Phys. Rev. Lett. **80**, 1121 (1998).

[14] A. Furusawa, J.L. Sorensen, S.L. Braunstein, C.A. Fuchs, H.J. Kimble, E.S. Polzik, Science **282**, 706 (1998).

[15] D. M. Greenberger, M. A. Horne, A. Zeilinger, Am. J. Phys. **58**, 1131 (1990).

[16] J. W.Pan, D. Bouwmeester, M. Daniell, H. Weinfurter, A. Zeilinger, Nature **403**, 515 (2000).

[17] D.M. Meekhof, C. Monroe, B.E. King, W.M. Itano and D.J. Wineland, Phys. Rev. Let., **76**, 1796 (1996).

[18] C.A. Sackett, D. Kielpinski, B.E. King, C. Langer, V. Meyer, C.J. Myatt, M. Rowe,Q.A. Turchette, W.M. Itano, D.J. Wineland, C.C. Monroe, Nature **404**, 256 (2000).

[19] S. Haroche and J.M. Raimond, Cavity Quantum Electrodynamics. *Scientific American* **268**, 54 (1993).

[20] R.G. Hulet and D. Kleppner, Phys. Rev. Lett. **51**, 1430 (1983). P. Nussenzveig, F. Bernardot, M. Brune, J. Hare, J.M. Raimond, S Haroche and W. Gawlik, Phys. Rev. A **48**, 3991 (1993).

[21] S. Haroche, in *Fundamental systems in quantum optics, les Houches Summer School Session LIII*, J. Dalibard, J.M. Raimond, and J. Zinn-Justin, eds. (North Holland, Amsterdam,1992), p. 767. S. Haroche, in *New Trends in Atomic Physics, les Houches Summer School Session XXXVIII*, G. Grynberg and R. Stora, eds. (North Holland, Amsterdam, 1984), p. 347.

[22] J.M. Raimond and S. Haroche, in *Quantum fluctuations, les Houches Summer School Session LXIII*, S. Reynaud E. Giaccobino and J. Zinn-Justin, eds. (North Holland, Amsterdam,1197), p. 309.

[23] S. Haroche and J.M. Raimond in *Avances in Atomic and Molecular Physics, supplement 2*, D. Bates and B. Bederson ed. (Academic Press, New York, 1985) p.347. S. Haroche and J.M. Raimond in *Avances in Atomic and molecular physics, supplement 2*, P. Berman ed. (Academic Press, New York, 1994) p.123.

[24] G. Raithel, C. Wagner, H. Walther, L.M. Narducci and M.O. Scully, Adv. At. Mol. Phys. (Supplement 2), 57 (1994).

[25] F. Bernardot, P. Nussenzveig, M. Brune, J.M. Raimond and S. Haroche, Euro. Phys. Lett. **17**,3 3 (1992).

[26] M. Brune, F. Schmidt-Kaler, A. Maali, J. Dreyer, E.Hagley, J.M. Raimond and S. Haroche, *Phys. Rev. Lett.* **76**, 1800 (1996).

[27] X. Maître, E. Hagley, G. Nogues, C. Wunderlich, P. Goy, M. Brune, J.M. Raimond and S. Haroche, *Phys. Rev. Lett.* **79**, 769 (1997).

[28] A. Rauschenbeutel, G. Nogues, S. Osnaghi, P. Bertet, M. Brune, J.M. Raimond and S. Haroche, Science, accepted (2000).

[29] M. Gross and J. Liang, Phys. Rev. Lett. **57**, 3160 (1986).

[30] G. Rempe, H. Walther and N. Klein, Phys. Rev. Lett,. **58**, 353 (1987).

[31] E.T. Jaynes and F.W. Cummings, Proc. IEEE, **51**, 89 (1963).

[32] C. Cohen-Tannoudji, J. Dupont-Roc and G. Grynberg, Photons et atomes, Introduction à l'électrodynamique quantique (Interéditions et Editions du CNRS 1987). English translation: Photons and Atoms, Introduction to Quantum Electrodynamics (Wiley, New York 1989).

[33] J.H. Eberly, N.B. Narozhny and J.J. Sanchez-Mondragon, Phys. Rev. Lett. **44**, 1323 (1980).

[34] R. Glauber, Phys. Rev. **131** 2766 (1963).

[35] B.T.H. Varcoe, S. Brattke and H. Walther, Nature, 403, 743-746 (2000).

[36] A. Auffeves, P. Maioli, T. Meunier, S. Gleyzes, G. Nogues, M. Brune, J. M. Raimond, and S. Haroche Phys. Rev. Lett. **91**, 230405 (2003)

[37] E. Hagley, X. Maître, G. Nogues, C. Wunderlich, M. Brune, J.M. Raimond and S. Haroche, Phys. Rev. Lett. **79**, 1 (1997).

[38] H. Rauch, A. Zeilinger, G. Badurek and A. Wilfing, Phys. Lett., **54 A**, 425 (1975).

[39] S.A. Werner, R. Colella, A.W. Overhauser and C.F. Eagen, Phys. Rev. Lett., **35**, 1053 (1975).

[40] G. Nogues, A. Rauschenbeutel, S. Osnaghi, M. Brune, J.M. Raimond and S. Haroche, Nature **400**, 239 (1999).

[41] A. Rauschenbeutel, G. Nogues, S. Osnaghi, P. Bertet, M. Brune, J.M. Raimond and S. Haroche, Phys. Rev. Lett. **83**, 5166 (1999).

[42] S. Haroche *et al.*, in Laser spectroscopy 14, R. Blatt, J. Eschner, D. Leibfried, F. Schmidt-Kaler eds. (World Scientific, New York, 1999) p. 140.

[43] S.B. Zheng, J. of Opt. B **1**, 534 (1999).

[44] S. Haroche, in Fundamental problems in quantum theory, D. Greenberger, A. Zeilinger, eds., Ann. N.Y. Acad. Sci. **755**, 73 (1995).

[45] B. T. H. Varcoe, S. Brattke, B.-G. Englert, H. Walther, in Laser spectroscopy 14, R. Blatt, J. Eschner, D. Leibfried, F. Schmidt-Kaler eds. (World Scientific, New York, 1999) p. 130.

[46] N. D. Mermin, Phys. Rev. Lett. **65**, 1838 (1990).

[47] N. A. Gershenfeld and I. L. Chuang, Science, **275**, 350, (1997); D. G. Cory, A. F. Fahmy and T. F. Havel, Proc. Natl. Acad. Sci. USA **94**, 1634 (1997); J. A. Jones, M. Mosca and R. H. Hansen, Nature **393**, 344 (1998); D. G. Cory et al, Phys. Rev. Lett. **81**, 2152 (1998).

[48] S.L. Braunstein, C.M. Caves, R. Jozsa, N. Linden, S. Popescu and R. Schack, Phys. Rev. Lett. **83**, 1054 (1999).

[49] C. Monroe, D.M. Meekhof, B.E. King, W.M. Itano and D.J. Wineland, Phys. Rev. Lett. **75**, 4714 (1995).

[50] Q. A. Turchette, C.S. Wood, B.E. King, C.J. Myatt, D. Leibfried, W.M. Itano, C. Monroe and D.J. Wineland, Phys. Rev. Lett. **81**, 3631 (1998).

[51] H. C. Nägerl, D. Leibfried, H. Rohde, G. Thalhammer, J. Eschner, F. Schmidt-Kaler, and R. Blatt, Phys. Rev. A **60**, 145 (1999).

[52] S. Osnaghi, P.Bertet, A. Auffeves, P. Maioli, M. Brune, J.M. Raimond, and S. Haroche, Phys. Rev. Lett.**87**, 037902 (2001).

[53] D. Jacksh, I. Cirac, P. Zoller, S. Rolston, R. Côté, M. Lukin,Phys. Rev. Lett. **85**, 2208 (2000).

[54] L. K. Grover, Phys. Rev. Lett.**79**, 325 (1997).

[55] F. Yamaguchi, P. Milman, M. Brune, J.-M. Raimond and S. Haroche,Phys. Rev. A **66**, 010302 (2002).

[56] M. lukin, M. Fleischhauer, R. Côté, L. Duan, D. Jacksch, I. Cirac and P.zoller, Phys. Rev. Lett. **87**, 037901 (2001).

[57] J. Reichel, W. Hänsel and T. W. Hänsch, Phys. Rev. Lett., **83**, 3398 (1999).

[58] M. Brune, E. Hagley, J. Dreyer, X. Maître, A. Maali, C. Wunderlich, J.M. Raimond and S. Haroche, Phys. Rev. Lett. **77**, 4887 (1996).

[59] We acknowledge support from the European Community and JST (ICORP “Quantum Entanglement" project).